International Journal of Intelligent Robotics and Applications
https://doi.org/10.1007/s41315-021-00171-6

REGULAR PAPER

Wind measurement by computer vision on unmanned sailboat

Dasheng Yang[1,2] · Zaisheng Pan[1,2] · Yan Cao[2] · Yifan Wang[3] · Xiao Lai[4] · Jian Yang[5] · Yong Liu[1]

Received: 15 October 2020 / Accepted: 30 March 2021

Abstract
The measurement accuracy of wind direction and wind speed is very important to the unmanned sailboat control, but the mature mechanical wind sensor and ultrasonic wind sensor both have great defects to be applied to the unmanned sailboat. Inspired by previous works on neural networks, we propose a low-cost, real-time, and robust wind measurement system based on computer vision (CV). This CV-wind-sensor includes an airflow rope and a camera, which can be simply deployed on the sailboat. We implement a prototype system on the FPGA platform and run a series of experiments that demonstrate the promising performance of our system. For example, the absolute measurement loss of the CV sensor in this paper is basically kept below 0.4 m/s, which shows a great advantage of measurement accuracy compared with the mechanical sensor.

Keywords Wind measurement · Unmanned sailboat · Applications of machine learning

1 Introduction

With the development of artificial intelligence technology and the maturity of global communication networks in recent years, the research on the ocean is gradually deepening, which requires real-time and long-term monitoring on ocean current, water quality and marine climate data. Because of its long endurance, flexible deployment and low maintenance cost, autonomous surface vehicle (ASV) (Cruz and Alves 2008; Rynne and von Ellenrieder 2008) especially unmanned sailboat is gradually applied in the field of environmental monitoring in the ocean, lakes, rivers, etc. (Manley 2008; Murphy et al. 2008; Pastore and Djapic 2010; Steimle and Hall 2006)

Similar to unmanned vehicles and unmanned aerial vehicles (UAVs), unmanned sailboats need to integrate multi-dimensional information such as geographical location, operation status, water environment, hull attitude, etc., and do autonomous navigation to complete the assigned operation tasks (Plumet et al. 2015). In order to realize the control algorithm efficiently and accurately, the sensing and measurement of various signals must be in high precision and real-time (Petres et al. 2011; Guo et al. 2011). Since the power of unmanned sailboats mainly comes from wind energy, the accuracy of the wind sensing directly determines the control efficiency.

In this paper, a wind measurement method for unmanned sailboat based on computer vision is presented. The measurement system is composed of an airflow rope, a camera and a computing platform, which can accurately measure the wind speed and direction by identifying the airflow rope's fluttering. Experiments show that this method not only improves the accuracy, and real-time performance of wind measurement on the unmanned sailboat but also reduces the installation cost.

✉ Yong Liu
yongliu@iipc.zju.edu.cn

Dasheng Yang
yangds@nz-ic.com

Zaisheng Pan
panzs@nz-ic.com

Yan Cao
caoyan@nz-ic.com

Yifan Wang
wangyifan@nz-ic.com

Xiao Lai
laixiao@supcon.com

Jian Yang
buaayangjian@126.com

[1] Zhejiang Universtiry, Hangzhou, China

[2] Ningbo SUPCON Microelectronics Co., Ltd, Ningbo, China

[3] Zhejiang Chipkong Technology Co., Ltd, Hangzhou, China

[4] ZheJiang SUPCON Technology Co., Ltd, Hangzhou, China

[5] China Research and Development Academy of Machinery Equipment, Beijing, China

Published online: 24 May 2021

2 Related work on wind sensing

At present, in the field of navigation, the measurement of wind speed and wind direction mainly depends on wind sensor. Dominating methods for this task can be roughly divided into three categories:

2.1 Mechanical wind sensor

Mechanical wind sensor includes cup anemometer Pindado et al. (2014), wind vanes Ebert and Wood (1995) and propeller anemometer SUZUKI et al. (1984), etc. A cup-vane wind sensor integrates a mechanical photoelectric conversion circuit which can calculate the rotation speed of the wind cup and the angle of the wind vane Kang'iri et al. (2018). The cost of the mechanical wind sensor is low, and the installation is simple. It has been widely used.

However, the accuracy of the mechanical wind sensor cannot be very high because its measurement results have a great relationship with its installation position. If it is installed on the top of the mast, due to the inclination of the ship during sailing, the sensor will also incline greatly, and the accuracy will be significantly reduced. If it is installed at the front or rear side of the deck, the turbulence of the sail will also seriously affect the accuracy. In addition, the response time of the mechanical sensor is too slow to provide a real-time control strategy Camp et al. (1970).

2.2 Ultrasonic wind sensor

Ultrasonic wind sensor measures wind's speed and direction by analyzing the modulation effect on ultrasonic by the passing airflow (Nakamura 2005; Svilainis and Dumbrava 2007; Quaranta et al. 1985). Ultrasonic wind sensor has rapid reaction speed, high measurement accuracy, no zero drift and longer service life. It has been widely used in large ships and marine equipment. Ultrasonic wind sensor also has its shortage. The inconstant wind and swinging of the boat may lead to errors in wind measurement Zhi-qian et al. (2020). Meanwhile, it is too large, too heavy and costs too much to be applied in the low-cost small unmanned sailboat.

Therefore, it is necessary to have a more economical and suitable wind direction and wind speed measurement technology in the unmanned sailboat.

2.3 Wind estimating based on machine learning

With the development of artificial intelligence technology, computer vision (CV) and machine learning technology have been gradually applied to the field of perception and measurement (Vodrahalli and Bhowmik 2017; Patruno et al. 2017).

Image or video data can be used to estimate the physical properties of fluid flows, such as flowing water (Spencer and Shah 2004; Mottaghi et al. 2016; Wu et al. 2016), or to estimate material properties of objects Meka et al. (2018) by extracting physical quantities from videos Bhat et al. (2003). There have been researches on estimating or forecasting wind speeds using time series of measurements from existing instrumentation or weather forecast data as inputs (Mohandes et al. 2014; Li and Shi 2010; Liu et al. 2018).

The present works aimed at wind speed regression from images or videos are based on previous studies on classifying videos by neural networks. Shubhi *et al.* Harbola and Coors (2019) propose two one-dimensional (1D) convolutional neural networks (CNN) for predicting dominant wind speed and direction whose accuracy reaches up to 95.2%. Runia *et al.* Runia et al. (2019) concentrate on flags curling in the wind and extract wind velocity and properties. Cardona *et al.* Cardona et al. (2019) demonstrate a coupled CNN and recurrent neural network architecture (RNN) that extracts the wind speed ranged from 0 to 15.5 m/s and encoded in visually recorded flow-structure interactions of a flag and tree in naturally occurring wind.

The related work above on estimating wind mostly focus on the fixed objects, such as wind power plants, trees or flags in the field. On the sailboat, the rapid movement, inclination of the sailboat and the change of the natural environment make the visual projection and fluid motion characteristics quite different from those works.

As shown in Fig. 1, in the actual navigation of a traditional sailboat, the sailor who is in charge of the sailing direction and speed usually quickly evaluates the wind speed and wind direction by observing the fluttering of airflow ropes on the sailboat, and then controls the sails considering the inclination angle and direction of the boat SU et al. (2014).

Therefore, this paper attempts to simulate the sailor's way of observing the airflow rope, estimating the wind direction

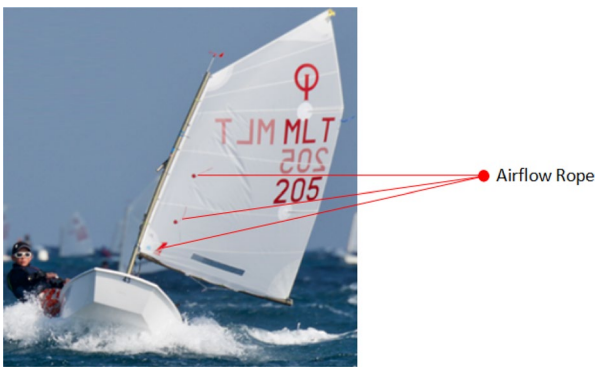

Fig. 1 Traditional sailboat with airflow ropes

and wind speed information by computer vision, and then realize the precise control of the unmanned sailboat.

3 Visual processing of airflow rope

The airflow rope will flutter under the wind, and a two-dimensional (2D) image which reflects the fluttering will be obtained by a camera installed under the airflow rope. Suppose there are n feature points on the image which are defined as $(X_0, Y_0, 1) \cdots \cdots (X_n, Y_n, 1)$. These feature points can be transferred into three-dimensional (3D) feature data through the camera's internal parameter matrix, the airflow rope's length, the installation height and other information from the structure. The transfer function can be described as:

$$\begin{bmatrix} x_n \\ y_n \\ z_n \end{bmatrix} = \begin{bmatrix} f_x & s & x_0 \\ 0 & f_y & y_0 \\ 0 & 0 & 1 \end{bmatrix}^{-1} * \begin{bmatrix} X_n \\ Y_n \\ 1 \end{bmatrix} \tag{1}$$

In this case, f_x and f_y are the camera's focal lengths, x_0 and y_0 are the main point coordinates of the image plane, s is the tilt parameter of the coordinate axis. The image information of a fluttering airflow rope is time-dependent, so the dynamic model of the airflow rope is established based on the combination of image frames of time t.

Under the wind, the sailboat will form a rolling angle φ (the angle between the X-axis of the boat and the horizontal plane) and a pitching angle ρ (the angle between the Y-axis of the boat and the horizontal plane), which will also affect the projection characteristics of airflow rope in the camera. However, the course angle of the boat(the angle of the hull around the Z-axis) has no effect on the projection features.

In general weather conditions, the wind's pitching angle is small ($< 5°$). In order to simplify the calculation, the pitching effect is ignored. That is, the z-axis component of the wind vector is 0. Thus the wind vector in the hull coordinate system is defined as $\begin{bmatrix} u \\ v \\ 0 \end{bmatrix}$, and the dynamic model $G(x)$ of the airflow rope is described as:

$$\begin{bmatrix} u \\ v \\ 0 \end{bmatrix} = G\left(\begin{bmatrix} x_0 & \cdots & x_n \\ y_0 & \cdots & y_n \\ z_0 & \cdots & z_n \end{bmatrix}, \begin{bmatrix} x_0^{-1} & \cdots & x_n^{-1} \\ y_0^{-1} & \cdots & y_n^{-1} \\ z_0^{-1} & \cdots & z_n^{-1} \end{bmatrix}, \ldots\ldots, \begin{bmatrix} x_0^{-t} & \cdots & x_n^{-t} \\ y_0^{-t} & \cdots & y_n^{-t} \\ z_0^{-t} & \cdots & z_n^{-t} \end{bmatrix}, \begin{bmatrix} \rho \\ \varphi \\ 0 \end{bmatrix}\right) \tag{2}$$

In this case, t is the time span of the image sequence, (x_n, y_n, z_n) is the relative 3D coordinate of feature point n, and $(x_n^{-1}, y_n^{-1}, z_n^{-1})$ is the relative 3D coordinate of feature point n in the previous frame.

In order to get the accurate wind speed and direction, it is necessary to get the wind vector in the geographical coordinate system instead of the hull coordinate system. So the transformation from hull coordinate system to geographic coordinate system is implemented. (q_0, q_1, q_2, q_3) are quaternions continuously updated by the First Order Runge–Kutta Method Shi and Liu (2019).

$$\begin{bmatrix} q_0 \\ q_1 \\ q_2 \\ q_3 \end{bmatrix}_{t+\Delta t} = \begin{bmatrix} q_0 \\ q_1 \\ q_2 \\ q_3 \end{bmatrix} + \frac{\Delta t}{2} \begin{bmatrix} -w_x q_1 - w_y q_2 - w_z q_3 \\ w_x q_0 + w_z q_2 - w_y q_3 \\ w_y q_0 - w_x q_1 + w_x q_3 \\ w_x q_0 + w_y q_1 - w_x q_2 \end{bmatrix} \tag{3}$$

By multiplying $\begin{bmatrix} u \\ v \\ 0 \end{bmatrix}$ with the inverse matrix of the direction cosine matrix CZhou et al. (2008), which represents the rotation direction of the hull body relative to the geographical coordinate system, the wind data in geographical coordinate system $\begin{bmatrix} U \\ V \\ 0 \end{bmatrix}$ can be obtained:

$$\begin{aligned} \begin{bmatrix} U \\ V \\ 0 \end{bmatrix} &= C^{-1} * \begin{bmatrix} u \\ v \\ 0 \end{bmatrix} \\ &= \begin{bmatrix} q_0^2 + q_1^2 - q_2^2 - q_3^2 & 2(q_1 q_2 + q_0 q_3) & 2(q_1 q_3 - q_0 q_2) \\ 2(q_1 q_2 - q_0 q_3) & q_0^2 - q_1^2 + q_2^2 - q_3^2 & 2(q_2 q_3 + q_0 q_1) \\ 2(q_1 q_3 + q_0 q_2) & 2(q_2 q_3 - q_0 q_1) & q_0^2 - q_1^2 - q_2^2 + q_3^2 \end{bmatrix}^{-1} \\ &\quad * G\left(\begin{bmatrix} x_0 & \cdots & x_n \\ y_0 & \cdots & y_n \\ z_0 & \cdots & z_n \end{bmatrix}, \begin{bmatrix} x_0^{-1} & \cdots & x_n^{-1} \\ y_0^{-1} & \cdots & y_n^{-1} \\ z_0^{-1} & \cdots & z_n^{-1} \end{bmatrix}, \ldots\ldots, \begin{bmatrix} x_0^{-t} & \cdots & x_n^{-t} \\ y_0^{-t} & \cdots & y_n^{-t} \\ z_0^{-t} & \cdots & z_n^{-t} \end{bmatrix}, \begin{bmatrix} \rho \\ \varphi \\ 0 \end{bmatrix}\right) \end{aligned} \tag{4}$$

And with the U and V obtained from (4), the wind speed and wind direction θ can be described as:

$$s = \sqrt{U^2 + V^2} \tag{5}$$

$$\theta = \tan^{-1} \frac{V}{U} \tag{6}$$

According to the above derivation, the wind speed and direction information can be calculated with the aerodynamic model of the airflow rope and IMU data. However, it is difficult to implement this method for two reasons.

First, it is difficult to extract features from the images. Even in the same circumstance, i.e., same wind speed and direction, the airflow rope may be in different forms, such as overlapping or bending. In addition, the environment light, contrast, background interference, etc. all increase the difficulty in extracting features.

Second, it is difficult to establish the aerodynamic model equation $G(x)$. Due to the material, weight, winding method, air humidity and other factors, the wind and airflow rope form a nonlinear system which is difficult to solve.

4 Wind sensor based on neural network

Because of the advantages in pattern recognition and nonlinear processing ability, machine learning based on CNN will be a good solution Szegedy et al. (2015) for the problems mentioned in Sect. 3.

4.1 Sensor structure

Under different wind direction and wind speed conditions, the characteristic image of airflow rope will be quite different. Fig. 2 shows four special cases.

In Fig. 2a, b show the status of the airflow rope in the crosswind from the side (same as X-axis direction of the hull). When the crosswind is weak, the rolling angle of the hull is small, and the airflow rope is blown up slightly, which forms a sinusoidal projection of the fluttering angle ω . With the increase of wind speed, the airflow rope is blown up more greatly, and the rolling angle of the hull φ is superposed to the fluttering angle and makes ω larger. When the wind speed is large enough, the airflow rope will be completely horizontal, and $\omega = \varphi + 90°$. When the wind speed continues increasing, the sinusoidal projection of ω becomes smaller due to the increase of φ. In other words,, the projection characteristics of the airflow rope are related to the wind speed and the roll angle ω.

Similarly, it can be seen from (c) and (d) that for the wind from the y-axis direction of the hull, the projection characteristics are related to the wind speed and the ship pitch angle ρ.

Thus, for the natural wind with different directions and speeds, the projection characteristics are strongly related to the wind , the pitching angle ρ and the rolling angle φ. That is to say, the wind vector $\begin{bmatrix} u \\ v \\ 0 \end{bmatrix}$ can be accurately calculated from projection features (camera data) and hull attitude $\begin{bmatrix} \rho \\ \varphi \\ 0 \end{bmatrix}$ (IMU data) theoretically.

Neural networks can be used for end-to-end training and inference. That is, the wind data can be directly calculated from the input of the camera and IMU. However, the end-to-end method which involves many conventional calculation processes in the network is difficult to train, particularly a much deeper network may be needed to obtain an accurate inference. This is not suitable for the embedded low-cost environment of unmanned sailboats.

Therefore, in this paper, the neural network is only used to deal with the non-linear part of the process, that is, the airflow rope dynamic model. The coordinate transformation and the solution of wind data are still completed by

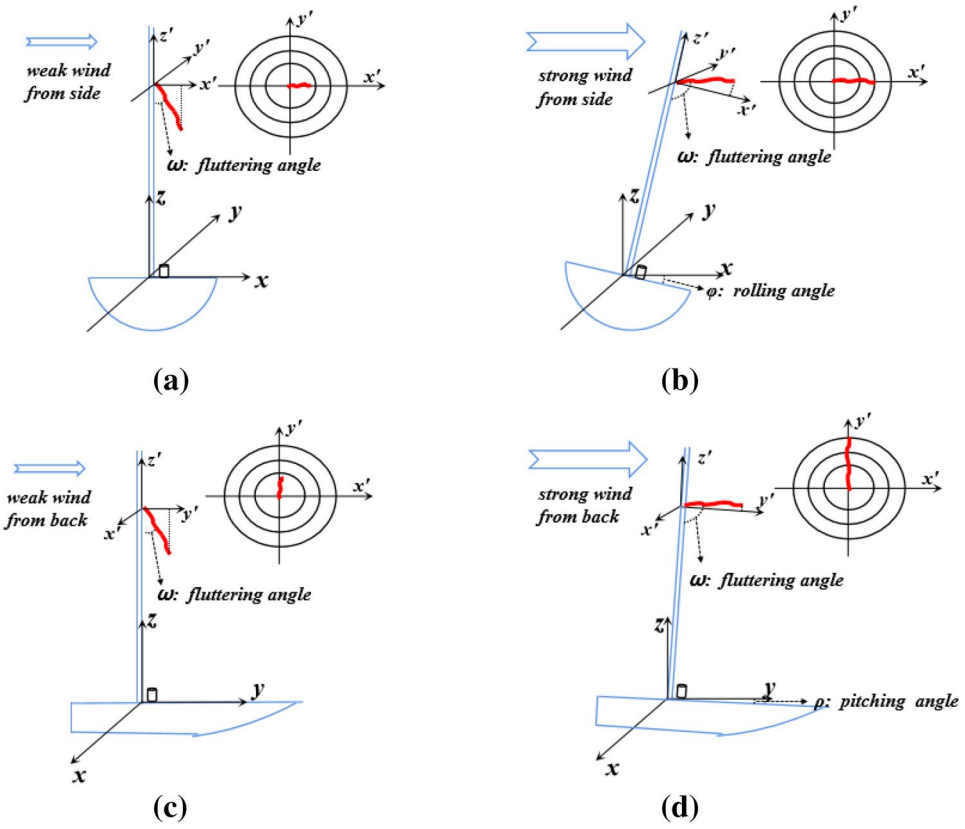

Fig. 2 **a**, **b** Show the status of the airflow rope in the crosswind from the left side. **c**, **d** Show the status of the airflow rope in the wind from back side

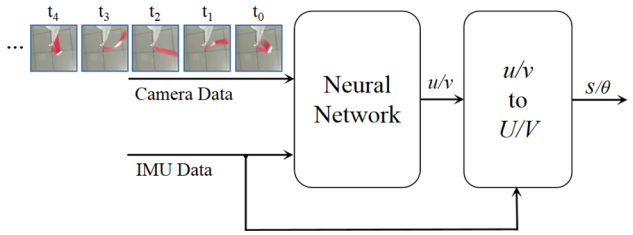

Fig. 3 Wind sensor structure with neural network

conventional mathematical calculation. The structure of this CV wind sensor is shown in Fig. 3.

4.2 Network model

As described in 4.1, The IMU data not only affects the conversion from $\begin{bmatrix} u \\ v \\ 0 \end{bmatrix}$ to $\begin{bmatrix} U \\ V \\ 0 \end{bmatrix}$, but also directly affects the measurement accuracy of $\begin{bmatrix} u \\ v \\ 0 \end{bmatrix}$. Therefore, it is necessary to construct a multi-source hybrid neural network by taking it as an input besides the image data. The two-stream convolutional networks proposed by Karen *et al.*Simonyan and Zisserman (2014) processes the optical flow and image stream separately, and then combined them by late fusion, which has proved a good effect in action recognition. This network provides an idea for this paper. However, one of inputs in our system is a one-dimensional data from IMU, and the other are 20 frames of 128*128 images. The large difference in the data amount between IMU and the camera may lead to improper weight training of the neural network, and cause the over-fitting problem. In fact, the wind can be roughly predicted only based on the camera data, so we assume that the effect of the camera data is greater than that of IMU. Therefore, we properly increase the dimension of IMU data to 8 to reduce the weight and increase its nonlinearity. At the same time, the dimension of video stream data is reduced, and these two-source data are then concatenated.

So in this article, a multi-source hybrid convolution neural network is constructed. The data is obtained from two sensors, i.e., the camera and the IMU installed on the boat. A branch convolution network processes the formatted video data acquired from the camera, and the other branch processes the boat hull angle data $\begin{bmatrix} \rho \\ \varphi \\ 0 \end{bmatrix}$ obtained from IMU. All channels will be concatenated in a full connection layer Tran et al. (2018). The controller of an unmanned sailboat cannot provide a strong computing environment with its embedded platform, so a shallow network will be more appropriate in this application to guarantee adaptability, reliability and efficiency. A 16-layer network is designed, whose structure is as shown in Fig. 4.

The result and label of this network are both vectors, so the distance of the vectors is defined as the loss function, that is, the square loss function. The function is described as:

$$L(Y, f(x)) = (Y - f(x))^2. \tag{7}$$

4.3 Data collection

In order to obtain a large number of stable and consistent data for network training and verification, an automatic data acquisition platform is built in a closed laboratory environment, which is composed of the wind generation device and data acquisition device.

The wind generation device is mainly composed of four electric fans around the boat, facing four directions. The wind speed is adjustable by the servos installed on fans. A programmed FPGA board controls each electric fan to blow wind in four strength levels and switches the level every 30 s. In this way, several groups of horizontal wind with different directions and speeds are generated to blow the airflow rope to flutter.

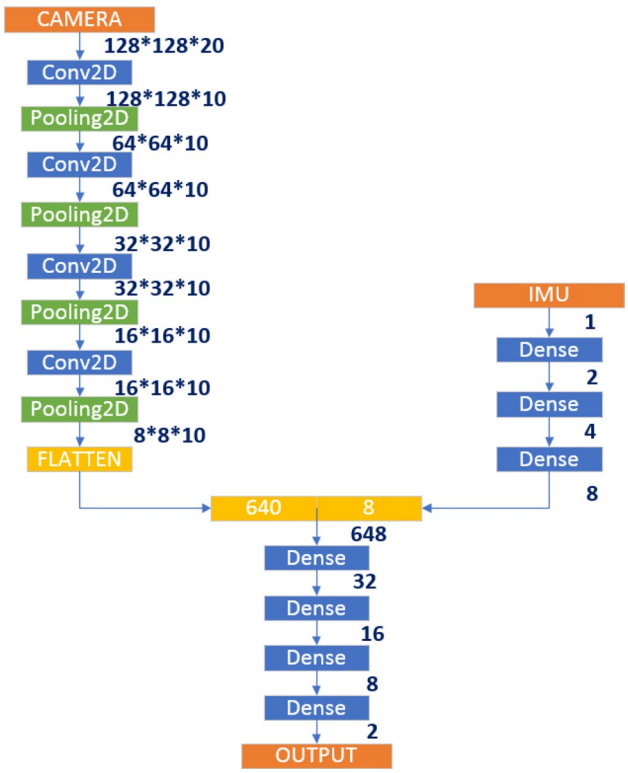

Fig. 4 Network structure

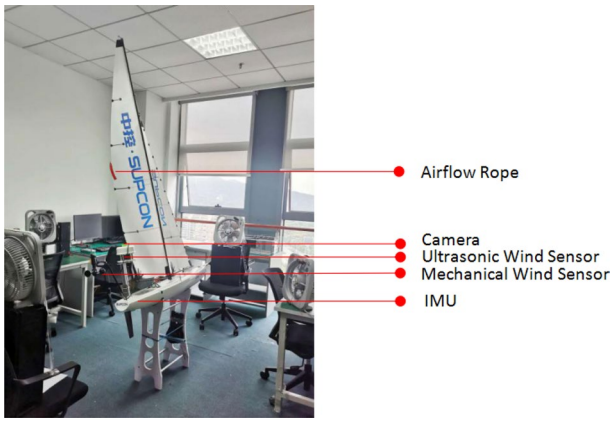

Fig. 5 Automatic data acquisition platform

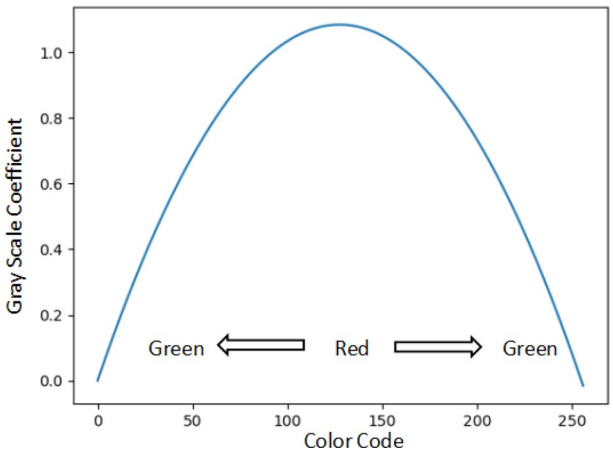

Fig. 6 The curve of gray scale coefficient

The data acquisition device consists of a servo motor installed at the bottom of the boat to control the inclination of the hull, a camera installed directly under the airflow rope, an IMU installed inside the boat, an ultrasonic wind sensor, and a mechanical wind sensor installed near the airflow rope (Fig. 5).

After the program is started, the FPGA board randomly controls four fan servos to generate a horizontal wind of random strength and direction. At the same time, the servo at the bottom of the boat is controlled to make the boat incline to the downwind direction. After waiting for 5 s when the wind is stable, the hull angle data $\begin{bmatrix} \rho \\ \varphi \\ 0 \end{bmatrix}$ will be obtained from IMU and a 20-frames-video data whose size is 20*640*480*3 will be obtained from the camera. The colorful image sequence data needs to be cleaned and normalized via square cutting, graying and scaling, etc., to generate 20*128*128*1 data.

Because the airflow rope is red, we hope to have a better response to red while keeping the response to all colors so as to get a greater anti-interference ability. Therefore the grayscale response function in this application is defined as:

$$f(h) = -h * (h - 255)/1500 \tag{8}$$

As shown in Fig. 6, after graying with this function, the red will be enhanced, while other colors will be attenuated. In order to enhance the model's resistance to interference, each sample will have a random gamma correction to simulate the visual effects of various lights.

The 20*128*128*1 matrix is regrouped to 20 channels, i.e. 1*128*128*20, and then combined with the hull angle data as the input of the network. At the same time, the current wind data $\begin{bmatrix} u \\ v \\ 0 \end{bmatrix}$ is obtained by ultrasonic wind sensor, which is used as the input. Save this data sample file and start the collection of the next sample.

For this application, a total of 100,000 groups of data samples are collected, 80% of which are randomly used as the training set, and the rest 20,000 groups are used as the test set.

4.4 Model training

We use Keras as the front end and Tensorflow as the back end for model training. And we implement the network on the PowerEdge R740 server, which is equipped with an Intel Xeon Silver 4214R processor and a GeForce GTX 1080Ti graphics card. Since the network model is a multi-input and single output model, the functional model structure of keras is chosen for the convenience of description. When training our model, we use Adam optimizer Kingma and Ba (2014) with a standard setting(i.e.,. a learning rate of 0.001, a first-moment momentum coefficient of 0.9, a second-moment momentum coefficient of 0.999). After 300 epochs, the training result is shown in Fig. 7.

As shown in Fig. 7, the average accuracy is 75% and the average loss of the wind speed is 0.13 m/s. We believe that under a more suitable network structure and more appropriate parameters configuration, the recognition accuracy can be greatly improved.

5 Experiment

5.1 Embedded environment implementation

As mentioned above, the unmanned sailboat is a relatively low-cost and low-performance embedded operating environment. In this paper, the unmanned sailboat controller is based on Xilinx XC7Z035 series FPGA chip, which is equipped with about 180K LUTs, a dual core

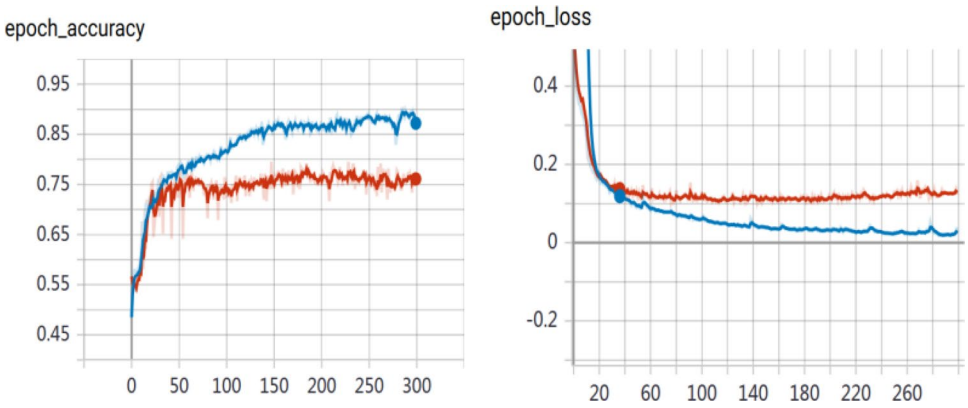

Fig. 7 Diagram of accuracy and loss vs. epoch. The red line shows the accuracy is up to 75% and the loss of the wind speed is less than 0.2 m/s after 50 epochs

cortex-A9 ARM processor and two 1GB DDR3 memories. So it is necessary to compress and accelerate the network, although it is already simple.

According to the designed network structure, we carry out the hardware acceleration on FPGA platform. A neural network co-processor module is developed, including 3*3 convolution operators, 2*2 max-pooling operators, full connection operators and common activation operators. All operators are based on semi-precision floating-point numbers, with an operating frequency of 100MHz. The structure of the module is shown in Fig. 8.

A program for network scheduling control is implemented, which organizes the data from DDR memory and sends them to the neural network co-processor module by Direct Memory Access (DMA). After the operation of the module, the result is sent back to DDR memory. According to the program, several DMA operations and data processing are carried out, and finally the results of the neural network are obtained. The conversion speed test denotes that it takes about 500ms to complete the conversion from the input and obtain the wind data, which meets the application requirement of unmanned sailboats.

5.2 Performance evaluation

In order to evaluate the performance of the network more directly, we compare the wind measurement effect to the mechanical sensor. Thus, besides the camera, the airflow rope and the control module as the tested equipment, an ultrasonic wind sensor and a mechanical wind sensor are also installed on the boat. The ultrasonic sensor is used as the measurement reference because of its high precision and fast response.

As shown in Fig. 9, the test environment is in a pool where there is a natural wind with random direction and speed. The measurement data of ultrasonic sensor, mechanical sensor and CV sensing system in this paper are together collected continuously. The geometric distance between the

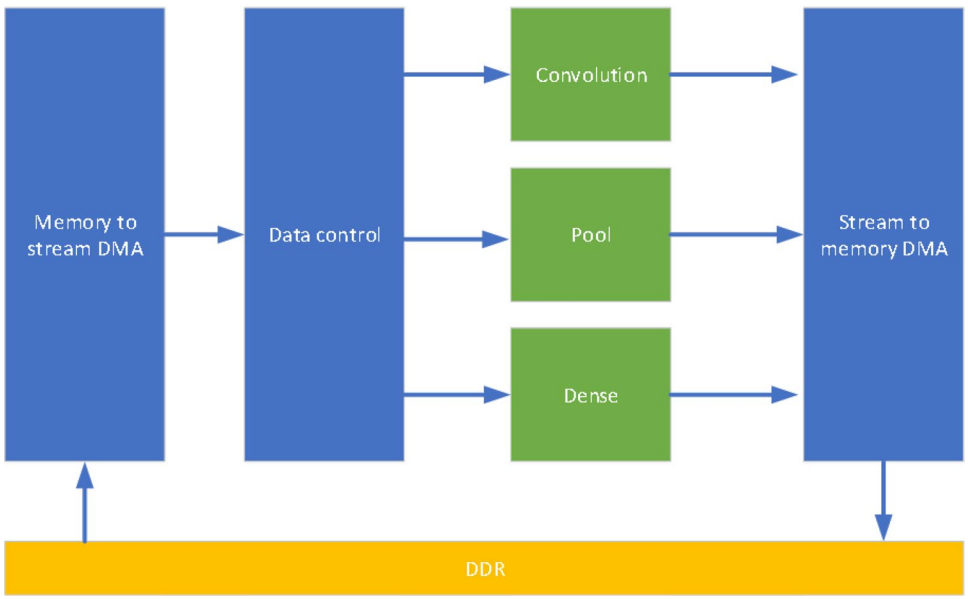

Fig. 8 The structure of the neural network co-processor module

measured data (velocity vector) of the tested sensor (i.e., the CV sensor in this paper and the mechanical sensor) and the ultrasonic sensor is calculated as the loss. The result, taking the measurement results of the ultrasonic sensor as a reference, is as follows.

As shown in Fig. 10, under common natural conditions where the wind speed is within 0–5 m/s,the measurement loss of the mechanical wind sensor is quite large. The loss is especially large when the wind is weak. When the wind's speed is about 3.5 m/s, the accuracy of the mechanical sensor is the highest, and then decreases again. There are several reasons for this. First, when the wind is weak and the wind changes its direction greatly or roughly turns around, the mechanical sensor's hysteresis phenomenon is serious, which needs more than 10 s to stable again. Second, when the wind is strong enough to make the boat tilt, the mechanical sensor will also have a pitching angle, which makes the measurement accuracy decline. The tilting effect varies with the wind, so the variance is large. The magnitude measurement loss of the mechanical sensor is larger than 0.4 m/s.

Fig. 9 The tested unmanned sailboat in pool

On the contrary, the magnitude measurement loss of the CV sensor in this paper is basically kept below 0.4m/s. When the wind's speed is about 1.5 m/s, the loss of the CV sensor is lowest, which is below 0.1 m/s. The loss and the variance also increase with the wind speed. When the wind's speed is larger than 3.5m/s, the airflow rope has been almost blown parallel to the horizontal plane, but the measurement is still relatively accurate.

We also did some experiments to evaluate the real-time performance.

As shown in Fig. 11, in the laboratory environment, after the wind direction suddenly changes by 90°, the deflection angles of the air flow rope and the wind vane are recorded. The response curves of the CV sensor and mechanical sensor to the wind changing are shown in Fig. 12.

When the wind changes, the airflow rope of the wind sensor and the wind vane of mechanical sensor will both have a hysteresis and then follow the change. The data

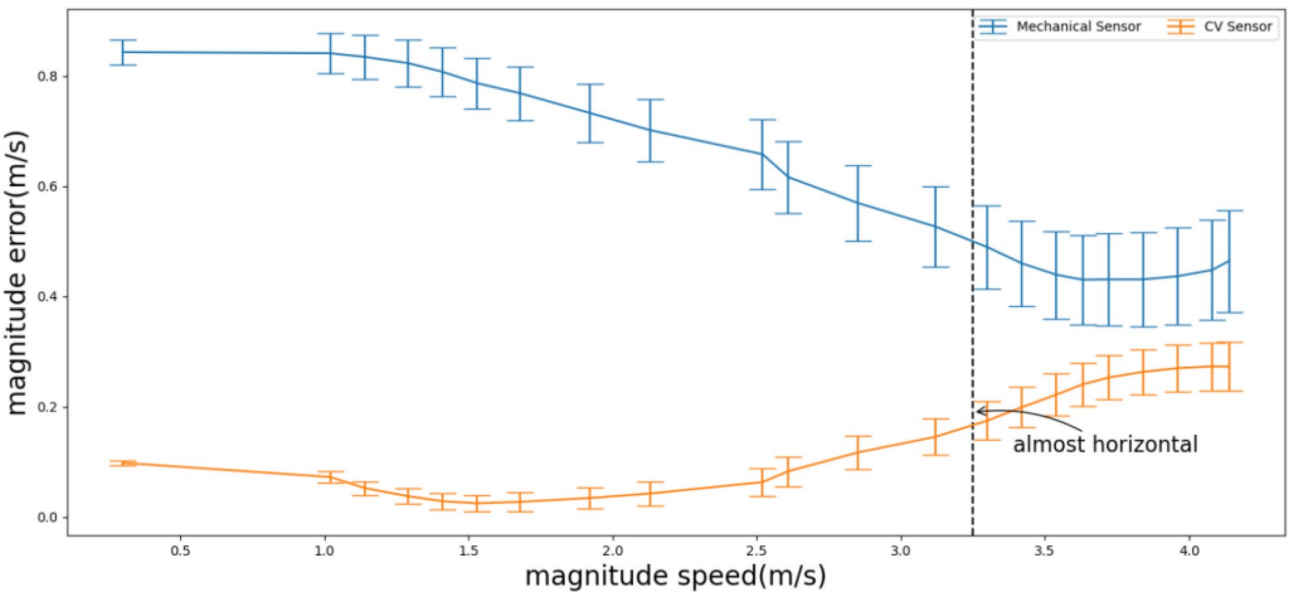

Fig. 10 The loss of CV sensor and mechanical sensor (ultrasonic sensor as reference). The airflow rope is parallel to the horizontal plane when the wind's speed is largerthan 3.5 m/s

collected in this hysteresis is inaccurate. Due to the lighter weight and softer material of the airflow rope, it's more sensitive to the wind changing, and the response is more timely. Figure 12 shows that when the wind changes instantaneously, the airflow rope can be stable again in about 0.6 s, while the wind vane will be stable gradually in more than 1.5 s. A shorter response time of the CV sensor means preciser data can be collected, which will be sent to the network accelerator to finish the conversation. It takes less than 1 s for the CV sensor to complete the measurement, which also makes the sensor more stable and real-time.

Due to the limitation of the natural environment, no data of wind speed above 4.5 m/s was collected. But from this test, the CV sensor still shows a great advantage of measurement accuracy compared with the mechanical sensor.

On the other hand, compared with the ultrasonic sensor, the CV sensor in this paper not only greatly reduces the implementation costs but also greatly reduces the load and space requirements of the unmanned sailboat due to its light and simple installation and deployment.

6 Conclusion

In this paper, we propose a wind measurement system based on CV, in which the nonlinear part of the airflow rope aerodynamic model is trained and replaced by the neural network. Experiments are conducted which demonstrate that the CV sensor has not only significant advantages in accuracy and real-time performance but also a low implementation cost and simple deployment, which is very suitable for unmanned sailboats.

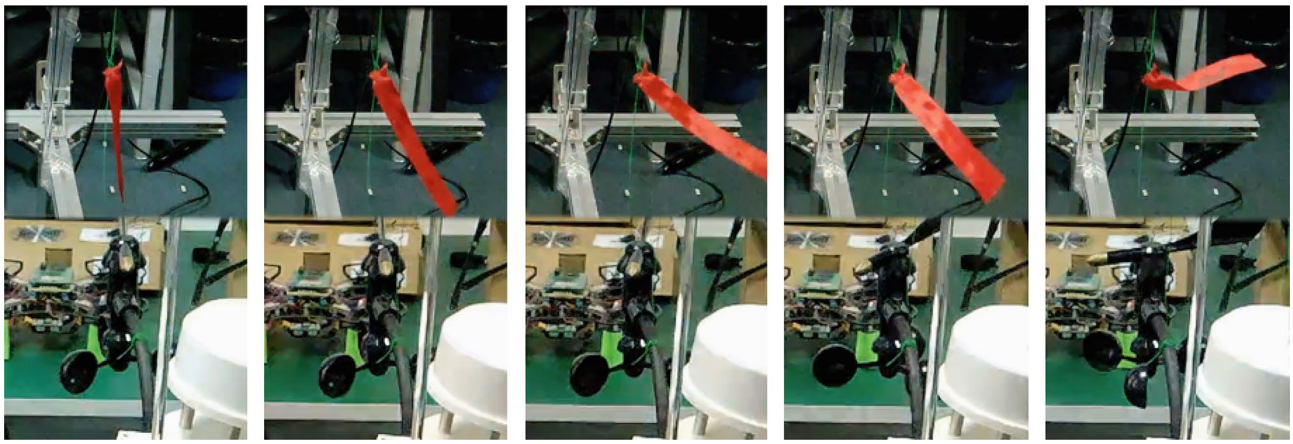

Fig. 11 The real-time performance experiment. When the wind suddenly changes, the airflow rope changes it's direction faster than the wind vane

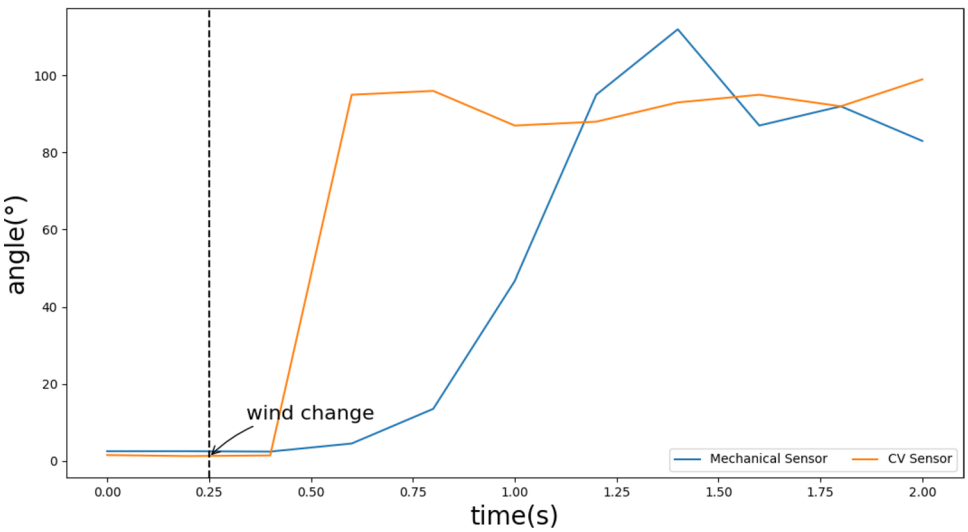

Fig. 12 Response of the CV sensor and mechanical sensor to the wind changing

Our CV wind sensor still has certain shortages. (1) The training data-set is collected in our laboratory environment, and takes the ultrasonic sensor as a reference, which cannot represent the real outdoor condition, especially the sea and the ocean. Besides, the inconstant wind and swinging of the boat may lead to errors in ultrasonic sensor measurement. For this problem, the same ultrasonic sensor whose position is fixed is used so that the bias caused by the reference can be neutralized as much as possible. Li's article Zhi-qian et al. (2020) also gives guidance on the correction method of ultrasonic wind sensors based on platform attitude. And in future researches, we will try to create a more accurate wind tunnel test environment, and use the standard wind data as the reference. (2) In this paper we only present a preliminary verification of the wind measurement based on CV. More researches on the neural network model and the airflow rope installation mode are needed to improve the measurement accuracy. For example, it is predictable to obtain higher measurement accuracy and robustness by installing airflow ropes in several key positions of the sailboat and evaluating the fluttering state of ropes with the same camera. In addition, the effect of different dimensions of IMU and camera data and the possible improper weight problem are also worthy of further research. (3) As mentioned, there are practical issues that impact the performance of our system (such as the precise position of the airflow rope and the camera). It will be a better solution for the final product to supply a fixed set of sensor kits and fine-tune a generic model for each boat.

References

Bhat, K.S., Twigg, C.D., Hodgins, J.K., Khosla, P.K., Popovic, Z., Seitz, S.M.: Estimating Cloth Simulation Parameters from Video. In D. Breen and M. Lin, editors, Symposium on Computer Animation. The Eurographics Association (2003)

Cardona, J.L., Howland, M.F., Dabiri, J.O.: Seeing the wind: Visual wind speed prediction with a coupled convolutional and recurrent neural network (2019)

Camp, D.W., Turner, R.E., Gilchrist, L.P.: Response tests of cup, vane, and propeller wind sensors. J. Geophys.. Res. **75**(27), 5265–5270 (1970)

Cruz, N.A., Alves, J.C.: Autonomous sailboats: An emerging technology for ocean sampling and surveillance. In: OCEANS 2008, 1–6 (2008)

Ebert, P.R., Wood, D.H.: On the dynamics of tail fins and wind vanes. J. Wind Eng. Industrial Aerodyn. **56**(2–3), 137–158 (1995)

Guo, Y., Romero, M., Ieng, S., Plumet, F., Benosman, R., Gas, B.: Reactive path planning for autonomous sailboat using an omnidirectional camera for obstacle detection. In: 2011 IEEE International Conference on Mechatronics, pages 445–450 (2011)

Harbola, S., Coors, V.: One dimensional convolutional neural network architectures for wind prediction. Energy Conversion Manag. **195**(SEP.), 70–75 (2019)

Kang'iri, S., Gradl, C., Byiringiro, J., Ngetha, H.: Design and calibration of a 3d-printed cup-vane wireless sensor node. Designs **2**(3), 21 (2018)

Kingma, D.P., Ba, J.: Adam: A method for stochastic optimization. arXiv preprint arXiv:1412.6980, (2014)

Liu, H., Mi, X., Li, Y.: Smart multi-step deep learning model for wind speed forecasting based on variational mode decomposition, singular spectrum analysis, lstm network and elm. Energy Conversion Manag. **159**(MAR.), 54–64 (2018)

Li, G., Shi, J.: On comparing three artificial neural networks for wind speed forecasting. Appl. Energy **87**(7), 2313–2320 (2010)

Manley, J.E.: Unmanned surface vehicles, 15 years of development. In: OCEANS 2008, 1–4 (2008)

Meka, A., Maximov, M., Zollhoefer, M., Chatterjee, A., Seidel, H. P., Richardt, C., Theobalt, C.: Live intrinsic material estimation, Lime (2018)

Mottaghi, R., Bagherinezhad, H., Rastegari, M., Farhadi, A.: Newtonian image understanding: Unfolding the dynamics of objects in static images. In: 2016 IEEE Conference on Computer Vision and Pattern Recognition (CVPR), pages 3521–3529 (2016)

Mohandes, M.A., Rehman, S., Halawani, T.O.: A neural networks approach for wind speed prediction. Renew Energy **13**(3), 345–354 (2014)

Nakamura, R.: Observational studies of stable nocturnal boundary layers: intermittent turbulence, sensible heat budgets and observational errors. (2005)

Murphy, R.R., Steimle, E., Griffin, C., Cullins, C., Hall, M., Pratt, K.: Cooperative use of unmanned sea surface and micro aerial vehicles at hurricane wilma. J. Field Robot. **25**(3), 164–180 (2008)

Patruno, C., Nitti, M., Stella, E., D'Orazio, T.: Helipad detection for accurate uav pose estimation by means of a visual sensor. Int. J. Adv. Robot. Syst. **14**(5), 1729881417731083 (2017)

Pastore, T., Djapic, V.: Improving autonomy and control of autonomous surface vehicles in port protection and mine countermeasure scenarios. J. Field Robot. **27**(6), 903–914 (2010)

Petres, C., Romero-Ramirez, M.-A., Plumet, F., Alessandrini, Bertrand: Modeling and reactive navigation of an autonomous sailboat. In: 2011 IEEE/RSJ international conference on intelligent robots and systems, pages 3571–3576. IEEE (2011)

Pindado, S., Cubas, J., Sorribes-Palmer, F..: The cup anemometer, a fundamental meteorological instrument for the wind energy industry. research at the idr/upm institute. Sensors **14**(11), 21418–21452 (2014)

Plumet, F., Pêtrès, C., Romero-Ramirez, M., Gas, B., Ieng, S.: Toward an autonomous sailing boat. IEEE J. Oceanic Eng. **40**(2), 397–407 (2015)

Quaranta, A.A., Aprilesi, G.C., De Cicco, G., Taroni, A.: A microprocessor based, three axes, ultrasonic anemometer. Journal of Physics E: Scientific Instruments **18**(5), 384 (1985)

Runia, T.F.H., Gavrilyuk, K., Snoek, C.G.M., Smeulders, A.W.M.: Go with the flow: perception-refined physics simulation (2019)

Rynne, P.F., von Ellenrieder, K.D.: A wind and solar-powered autonomous surface vehicle for sea surface measurements. In: OCEANS 2008, 1–6 (2008)

Simonyan, K., Zisserman, A.: Two-stream convolutional networks for action recognition in videos. Adv. Neural Inform. Process. Syst. **1**, 06 (2014)

Shi, K., Liu, M.: Strapdown inertial navigation quaternion fourth-order runge-kutta attitude algorithm. J. Detection Control **041**(003), 61–65 (2019)

Spencer, L., Shah, M.: Water video analysis. In: 2004 International Conference on Image Processing, 2004. ICIP'04., volume 4, pages 2705–2708. IEEE (2004)

Steimle, E.T., Hall, M.L.: Unmanned surface vehicles as environmental monitoring and assessment tools. In: OCEANS 2006, 1–5 (2006)

Suzuki, T., Kamano, T., Harada, H.: Study on characteristics of a propeller type anemometer. Wind Engineers. JAWE **1984**(22), 5–12 (1984)

Su, F., Shang, D.-z., Wang, J.-b., Liu, X.-m., Zhu, Q.: Sports Center Aquatic. A measurement method of sailing attitude based on mems gyroscope and accelerometer. J Terahertz Sci Electron Inform Technol (2):9 (2014)

Svilainis, L., Dumbrava, V.: Measurement of complex impedance of ultrasonic transducers. Ultragarsas'' Ultrasound'' **62**(1), 26–29 (2007)

Szegedy, C., Liu, W., Jia, Y., Sermanet, P., Reed, S., Anguelov, D., Erhan, D., Vanhoucke, V., Rabinovich, A.: Going deeper with convolutions. In: Proceedings of the IEEE conference on computer vision and pattern recognition, pages 1–9 (2015)

Tran, D., Wang, H., Torresani, L., Ray, J., LeCun, Y., Paluri, M.: A closer look at spatiotemporal convolutions for action recognition. In: Proceedings of the IEEE Conference on Computer Vision and Pattern Recognition (CVPR), June (2018)

Vodrahalli, K., Bhowmik, A.K.: 3d computer vision based on machine learning with deep neural networks: A review. Journal of the Society for Information Display **25**(11), 676–694 (2017)

Wu, J., Lim, J. J., Zhang, H., Tenenbaum, J.B., Freeman, W. T.: Physics 101: Learning physical object properties from unlabeled videos. In: British Machine Vision Conference (2016)

Zhi-qian, L., Ni, W., Sui-ping, Q., Zhi-wei, Z., Jia, S., Dong-ming, W.: Research on correction method of wind measurement based on platform attitude. In: Journal of Physics: Conference Series, volume 1607, page 012073. IOP Publishing (2020)

Zhou, S., Cong, Y., Li, J., Dai, H.: Comparison of algorithms for extracting quaternion from dcm. J. Chinese Inertial Technol. **016**(004), 415–418 (2008)

Dasheng Yang received the B.E. degree and M.E. degree from Zhejiang University, China, in 2004 and 2018, respectively, where he is currently pursuing the Ph.D. degree. His current research interests include Industria AI, Intelligent Control, and Control Module on Chip (CMC Chip). Mr. Yang is a senior engineer, and a member of the China National Standardization Technical Committee.

Zaisheng Pan received the B.E. degree in production process automation (automation) and the M.E. degree in industrial automation from Zhejiang University, in 1993 and 1996, respectively. He is a senior engineer. Since April 1996, he has been in the Department of Control Science and Engineering, Zhejiang University, where he engages in scientific research and product development.

Yan Cao received the B.E. degree from Northeastern University, China and M.E. degree from Zhejiang University, China , in 2007 and 2016, respectively. His current research interests includes intelligent control of USV. He is a senior engineer who completed the mathematical modeling in this article.

Yifan Wang received the B.E. degree in automation from Dalian Jiaotong University, China in 2017. He is a engineer on SoC and AI algorithm in Zhejiang Chipkong Technology Co.,Ltd, China. He did the algorithm validating work in this article.

Xiao Lai received the M.E. degree from Zhejiang University, China in 2011. She is a senior engineer. She is currently a manager on researching in ZheJiang SUPCON Technology Co.,Ltd, China. Mrs. Lai is the director of Automation Branch of China Instrument Industry Association.

Jian Yang received the B.S. degree and the Ph.D. degree from Beihang University, Beijing, China, in 2002 and 2008, respectively. He is currently a Researcher at China Research and Development Academy of Machinery Equipment, Beijing, China. His current research interests include robotics and information fusion.

Yong Liu received his B.S. degree and the Ph,D. degree from Zhejiang University, in 2001 and 2007, respectively. He is currently a professor in the institute of Cyber Systems and Control, Zhejiang University. He has published more than 30 research papers in machine learning, computer vision, information fusion. His latest research interests include machine learning, robotics vision, information processing and granular computing.